Dynamics of a polymer chain in an elongational flow

T. Hofmann, R. G. Winkler, and P. Reineker
Abteilung Theoretische Physik, Universität Ulm, D-89069 Ulm, Germany
(Received 17 September 1999)

The configurational and rheological properties of a flexible polymer chain in an elongational flow are studied analytically. To take into account the finite extensibility of a linear chain molecule, we apply the constraint of a fixed contour length, which leads to deformation dependent force coefficients. For the steady state, the distribution and partition functions are calculated using the maximum entropy approach. A comparison of our predictions for the strain rate dependence of the deformation and the intrinsic viscosity with computer simulations yields good agreement. Furthermore, we analyze the dynamics of the polymer chain for different nonequilibrium initial conformations by solving the Langevin equation. In this case the time to approach the steady state depends upon the chosen initial conformation.

PACS number(s): 61.25.Hq, 36.20.Ey, 83.10.Nn

I. INTRODUCTION

The behavior of dilute polymer solutions in an elongational flow has been an outstanding problem in polymer science for several decades [1–6], both from experimental and theoretical points of view. The velocity gradient along the direction of flow can stretch the polymer far from its equilibrium configuration. Due to the extension, the polymer exerts a force back on the solvent that leads to important non-Newtonian properties of the solution such as turbulent drag reduction or enhancement of the solution viscosity [5,7]. For a theoretical description, the hydrodynamic interaction mediated by the solvent combined with the nonequilibrium state of the chain causes major problems. Thus, for an analytical approach, simple models are required which still capture the basic features of a polymer chain. Many theories use the Rouse model or the dumbbell model to describe the polymer chain. The major advantage of these models is analytical tractability, although they possess major drawbacks too, since all nonlinear effects like the finite extensibility [5,8–10] or the hydrodynamic interaction [11–13], as well as the excluded volume interaction, are neglected. The three above mentioned effects differ in their importance for the conformational and rheological properties of a polymer chain in an elongational flow. Due to the extension of a chain by the flow, the finite extensibility of a real polymer chain is of fundamental importance for the actual conformation of the chain because it yields a serious constraint for the deformation of the chain. On the other hand, the influence of the excluded volume effect should be negligible, especially for high strain rates, since it decreases with increasing segment-segment distance. The hydrodynamic interaction, however, is long ranged in nature, and its influence on the chain conformation and dynamics does not vanish with increasing chain extension.

So far we addressed the steady state properties of a chain in a flow field. However, because of the limited residence time of a polymer in a flow field, the steady state is rarely reached in experiments [14,15]. Thus it is of paramount importance to describe the dynamic properties of the chain as well. Unfortunately, up to now most theoretical descriptions are only applicable for the calculation of steady state properties of a chain.

In this paper we present an analytical description of the steady state as well as non-steady-state properties of a polymer chain in an elongational flow. In particular, we take into account the finite chain extensibility by constraints. The hydrodynamic interaction is neglected in the following calculation. Its influence on the chain conformations and dynamics will be discussed in a future publication. In addition, the excluded volume interaction is neglected (see the comment above). Comparisons of our results with computer simulations will be presented. In particular, our method allows one to calculate the residence time dependence of the mean square end-to-end distance for different nonequilibrium initial conformations. Predictions for this dependence for initially coiled or stretched chains, respectively, are in good agreement with recent computer simulations [16,17]. Our results show that the time to approach the steady state depends upon the chosen initial conformation.

The paper is organized as follows. In Sec. II the chain model is described. In Sec. III the steady state properties are discussed. The strain rate dependence of the mean square end-to-end distance and the intrinsic viscosity are calculated and compared to the predictions of computer simulations. In Sec. IV we outline our approach to calculate the nonequilibrium dynamics of the polymer chain in an elongational flow. Solutions of the equations of motion are presented for two distinct nonequilibrium initial conformations of the chain (coiled and stretched) and are compared with computer simulations. Finally, Sec. V summarizes our results.

II. MODEL

The polymer chain is comprised of $N+1$ identical mass points of mass m. The positions of the points are given by $\mathbf{r}_n, n=0,1,\ldots,N$. Furthermore we use the center of mass reference frame, i.e., $\Sigma_{n=0}^{N}\mathbf{r}_n=0$ for the calculation of the steady state properties. The bonds between successive mass points are taken into account in a mean field description by the constraints

$$\langle(\mathbf{r}_n-\mathbf{r}_{n-1})^2\rangle=l^2, \quad n=1,\ldots,N, \tag{1}$$

where l^2 is the mean square distance between successive mass points. These constraints guarantee the finite extensibility of the chain. Using the maximum entropy principle [18–21], the distribution function

$$\psi(\{\mathbf{r}_n\}) = \frac{1}{Z}\exp\left(-\frac{1}{l^2}\sum_{n=1}^{N} \nu_n(\mathbf{r}_n-\mathbf{r}_{n-1})^2 \right) \times \exp[-\beta V(\{\mathbf{r}_n\})]\,\delta\left(\frac{1}{N+1}\sum_{n=0}^{N} \mathbf{r}_n \right) \tag{2}$$

and the partition function

$$Z = \int d^{3(N+1)}r \exp\left(-\frac{1}{l^2}\sum_{n=1}^{N} \nu_n(\mathbf{r}_n-\mathbf{r}_{n-1})^2 \right) \times \exp[-\beta V(\{\mathbf{r}_n\})]\,\delta\left(\frac{1}{N+1}\sum_{n=0}^{N} \mathbf{r}_n \right) \tag{3}$$

can easily be calculated, where V denotes an external potential. The Lagrangian multipliers ν_n take the constraints (1) into account, and are determined by

$$1 = -\frac{\partial}{\partial \nu_n}\ln Z, \quad n=1,\ldots,N. \tag{4}$$

For an elongational flow, the external potential V is given by

$$V(\{\mathbf{r}_n\}) = -\frac{\zeta}{2}\sum_{n=0}^{N} \mathbf{r}_n \boldsymbol{\kappa} \mathbf{r}_n, \tag{5}$$

where

$$\boldsymbol{\kappa} = \begin{pmatrix} -\dot{\epsilon}/2 & 0 & 0 \\ 0 & -\dot{\epsilon}/2 & 0 \\ 0 & 0 & \dot{\epsilon} \end{pmatrix} \tag{6}$$

is the rate of deformation tensor, and ζ is the friction coefficient of a single bead (for details on elongational flows, see Refs. [5,22]). For this choice of the strain rate tensor the flow has a stagnation point at $\mathbf{r}=\mathbf{0}$. The calculation of the Lagrangian multipliers according to Eq. (4) leads to a set of N nonlinear coupled equations which cannot be solved analytically. To obtain analytical solutions for the Lagrangian multipliers as well as for certain ensemble averages (see below), a simplification is required.

III. STEADY STATE PROPERTIES

In this section we will calculate the steady state properties of the polymer chain. As already mentioned above, the equations of our model are not analytically tractable. Therefore, we will present two different approaches in this section. In Sec. III A we are interested in analytical solutions, which require a simplification of our model. In Sec. III B the numerical solution of the model is presented without any simplification as well as a comparison between the analytical results of the simplified model with the numerical solution of the full problem.

A. Analytical solution

The equations for the steady state can be solved analytically if we assume that all the Lagrangian multipliers are equal, i.e.,

$$\nu_n = \nu_m = \nu, \quad \forall n,\ m=1,\ldots,N. \tag{7}$$

Physically this means that all segments along the chain are considered identical. The N constraints of Eq. (1) are now reduced to a single constraint

$$\sum_{n=1}^{N} \langle (\mathbf{r}_n-\mathbf{r}_{n-1})^2 \rangle = N l^2. \tag{8}$$

Notice that the single constraint of Eq. (8) guarantees the finite extensibility of the chain as a whole, but allows for an inhomogeneous stretching of the bonds along the chain contour. As a consequence, some bonds of the chain may be longer than others in the ensemble average. This is in contrast to the original constraints of Eq. (1), where all bonds are required to be of the same length in the ensemble average.

Using the constraint described by Eq. (8), a normal mode transformation according to

$$\mathbf{r}_n = \sqrt{\frac{2}{N+1}}\sum_{k=0}^{N} \boldsymbol{\chi}_k \cos\left[\frac{k\pi}{N+1}\left(n+\frac{1}{2} \right) \right] \tag{9}$$

yields the partition function [Eq. (3)]

$$Z \sim \prod_{k=1}^{N} \left[\left(\frac{\pi}{\frac{2\nu}{l^2}\left(1-\cos\frac{k\pi}{N+1} \right) + \frac{\beta\zeta}{4}\dot{\epsilon}} \right) \times \left(\frac{\pi}{\frac{2\nu}{l^2}\left(1-\cos\frac{k\pi}{N+1} \right) - \frac{\beta\zeta}{2}\dot{\epsilon}} \right)^{1/2} \right] \tag{10}$$

in the center of mass reference frame ($\boldsymbol{\chi}_0=0$). Using $N l^2 = -\partial \ln Z/\partial \nu$, the Lagrangian multiplier follows from

$$N = \frac{1}{\nu}\left\{ N - \tanh\frac{\mu}{2}[(N+1)\coth(N+1)\mu - \coth\mu] \right\} + \frac{1}{2\nu}\left\{ N - \tan\frac{\varphi-\pi}{2}[(N+1)\cot(N+1)(\varphi-\pi) - \cot(\varphi-\pi)] \right\}, \tag{11}$$

with $\cosh\mu = 1+\tilde{\dot{\epsilon}}/(8\nu)$ and $\cos\varphi = \tilde{\dot{\epsilon}}/(4\nu)-1$. In Eq. (11) we introduced the scaled deformation rate $\tilde{\dot{\epsilon}} = \tau\dot{\epsilon}$, with

$$\tau = \frac{\zeta l^2}{k_B T}. \tag{12}$$

The strain rate dependence of the Lagrangian multiplier cannot be calculated analytically from Eq. (11); therefore, we have to solve this equation numerically for every strain rate.

The shape of a polymer chain can be described by the mean square end-to-end distance or the radius of gyration. Using the stationary state distribution function [Eq. (2)], the ensemble averages for the mean square end-to-end distance and the radius of gyration can be calculated in a straightforward manner, and we obtain

$$\langle (x_N - x_0)^2 \rangle = \frac{l^2}{2\nu} \left(\coth\frac{\mu}{2} \tanh\frac{N+1}{2}\mu - 1 \right), \tag{13}$$

$$\langle (z_N - z_0)^2 \rangle = \frac{l^2}{2\nu} \left(\cot\frac{\varphi-\pi}{2} \tan\frac{N+1}{2}(\varphi-\pi) - 1 \right), \tag{14}$$

$$R_G^2 = \frac{l^2[(N+1)\coth(N+1)\mu - \coth\mu]}{2\nu(N+1)\sinh\mu} - \frac{l^2[(N+1)\cot(N+1)(\varphi-\pi) - \cot(\varphi-\pi)]}{2\nu(N+1)\sin(\varphi-\pi)}, \tag{15}$$

where ν is determined from Eq. (11) (for symmetry reasons, the y component of the mean square end-to-end distance is identical with the x component). Figures 1 and 2 show the strain rate dependence of the mean square end-to-end distance and the radius of gyration in comparison to computer simulation data [16,23]. According to Fig. 1, significant chain stretching occurs only at strain rates above $\dot{\tilde{\epsilon}} \approx \dot{\tilde{\epsilon}}_c = 3\pi^2/N^2$. It should be noted that the simple Rouse model (where $\nu = 3/2$ for all strain rates) diverges at this point. Our predictions for the strain rate dependence of the mean square end-to-end distance and of the radius of gyration agree well with computer simulation results for low and moderate strain rates, whereas for high strain rates we find a discrepancy of about 10% between our data and the computer simulation data. This discrepancy is explained by the fact that in the computer simulations a bead-rod model is used, whereas we use a modified bead-spring model. In the bead-rod model all bonds along the chain remain unstretched for all strain rates. Conversely, in our bead-spring model the constraint of Eq. (8) allows for the stretching of some bonds along the chain as long as the sum over all squared distances between successive beads remains constant in the ensemble average. A closer examination indeed shows that the bonds in the middle of the chain are stretched compared to the bond length of the bead-rod model. In order to compensate for that stretching, the bonds at the chain ends are shorter in average. Figure 3 shows the bond length dependence along the chain for various strain rates. Obviously, the discrepancies between the lengths of the bonds at the chain ends and those in the middle increases with increasing strain rate. Thus it can be expected that our model disagrees with computer simulations of a bead-rod chain for high strain rates. Moreover, Fig. 1 shows that even for very high strain rates the rod limit is not reached. Our model predicts a maximum mean square end-to-end distance of about 80% of the rod limit. Nevertheless, our simplified analytical calculations capture the basic features of polymer chains exposed to an elongational flow. For strain rates above the coil-stretch transition ($\dot{\tilde{\epsilon}} \approx 3\pi^2/N^2$), we are able to find approximate solutions for Eqs. (13)–(15).

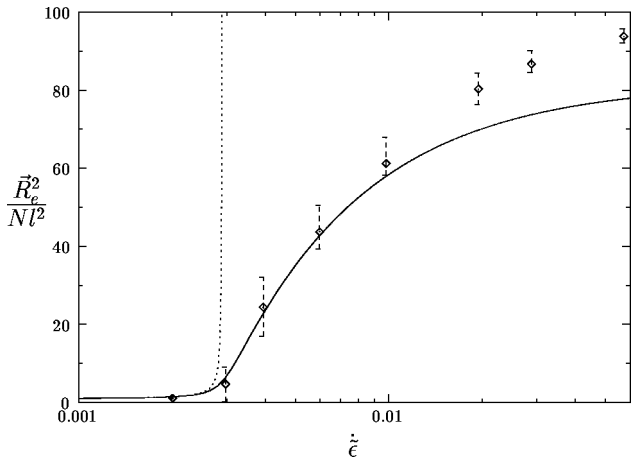

FIG. 1. Elongational rate dependence of the mean square end-to-end distance for an $N = 100$ chain determined by Eq. (13) (solid line). The dashed curve shows the results of the Rouse model. The single points are given by a computer simulation of a bead-rod chain [16].

For such strain rates the Lagrangian multiplier ν is proportional to the strain rate, and Eq. (11) yields $\nu = N^2\dot{\tilde{\epsilon}}/(2\pi^2)$. Inserting this approximation, we obtain

$$\langle (\mathbf{r}_N - \mathbf{r}_0)^2 \rangle = \frac{8N^2l^2}{\pi^2}\left(1 - \frac{3\pi^2}{\dot{\tilde{\epsilon}}N^2}\right),$$

$$R_G^2 = \frac{N^2l^2}{\pi^2}\left(1 - \frac{3\pi^2}{\dot{\tilde{\epsilon}}N^2}\right) \tag{16}$$

for strain rates $\dot{\tilde{\epsilon}} > 3\pi^2/N^2$. These approximate solutions reproduce the exact numerical values very accurately. From Eqs. (16) we find the maximum value

$$\lim_{\dot{\tilde{\epsilon}}\to\infty} \langle (\mathbf{r}_N - \mathbf{r}_0)^2 \rangle = \frac{8N^2l^2}{\pi^2} \approx 0.81N^2l^2 \tag{17}$$

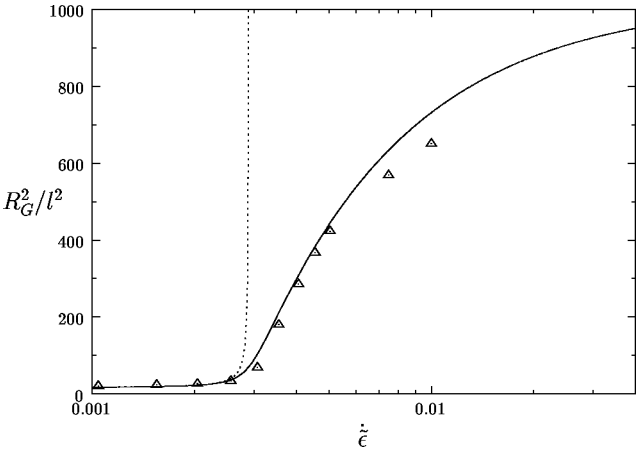

FIG. 2. Radius of gyration vs elongational rate for our theoretical predictions (solid line), the Rouse model (dashed line), and computer simulations [23] (points) for a chain with $N = 100$ beads.

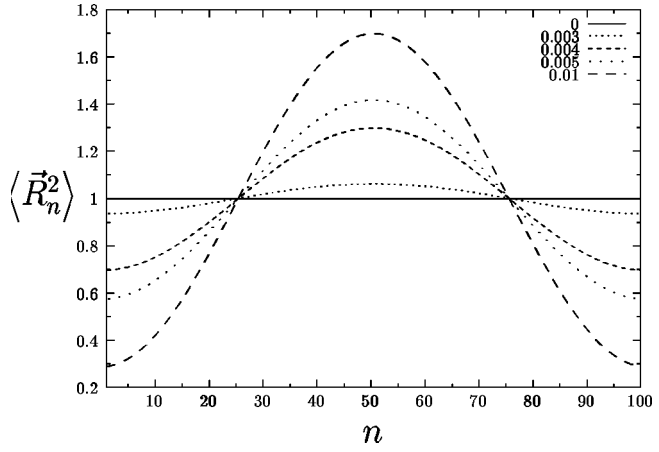

FIG. 3. Mean square extension of individual bonds as a function of the position along the chain for a chain with $N=100$ beads. The various curves display different strain rates, starting at $\dot{\tilde{\epsilon}}=0$ (no flow) up to $\dot{\tilde{\epsilon}}=0.01$ representing a highly stretched conformation.

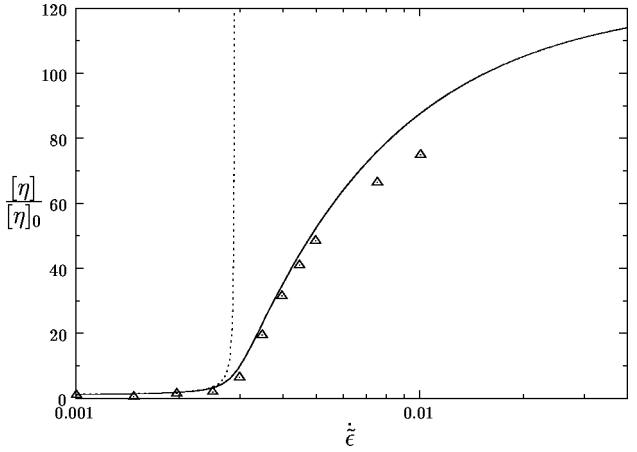

FIG. 4. Intrinsic viscosity as a function of the elongational rate calculated from Eq. (19) (solid line). The results of the Rouse model (dashed line) and a computer simulation [23] (points) are provided for comparison. The chain length is $N=100$.

for the end-to-end-distance of our model. Notice, that the strain rate dependent term of Eqs. (16) is independent of the chain length. Hence we obtain universal behavior with respect to changes in the chain length, if we scale the end-to-end distance or the radius of gyration by the square of the chain length ($L=Nl$) and the strain rate by the Rouse relaxation time τ_R given by

$$\tau_R=\frac{N^2 l^2 \zeta}{3\pi^2 k_B T}, \tag{18}$$

respectively. A numerical calculation indeed shows that the differences between these quantities at a given strain rate $\dot{\tilde{\epsilon}}$ vanish with increasing chain length. Therefore, we limit our further calculations to relatively short chains of $N=100$, because a further increase of the chain length yields no significant new results.

According to Eq. (13), the x and y components of the end-to-end distance approach zero with increasing strain rate. Hence, the chain is not only highly stretched in an elongational flow but also highly oriented.

In addition, we calculated the intrinsic elongational viscosity for the steady state, which characterizes the rheological properties of the solution. For bead-spring models the intrinsic viscosity is given [22,24]

$$\frac{[\eta]}{[\eta]_0}=\frac{12}{N}\left(\frac{1}{2}R_{G,x}^2+R_{G,z}^2\right), \tag{19}$$

where $[\eta]_0$ is the viscosity for $\dot{\tilde{\epsilon}}=0$. The strain rate dependence of the intrinsic viscosity of Fig. 4 exhibits a qualitative similar behavior as the one for the end-to-end distance or the radius of gyration. Below a critical strain rate the intrinsic viscosity remains virtually constant. Above $\dot{\tilde{\epsilon}}_c$ the intrinsic viscosity increases rapidly, and reaches a stationary value far above the equilibrium value at high strain rates. Again, the intrinsic viscosity calculated by the Rouse model diverges above the critical strain rate. Similar to the end-to-end distance and the radius of gyration, a good agreement with computer simulations [23] is achieved for low and moderate strain rates. For high strain rates, we again find a discrepancy of approximately 10%, which can be explained by the differences of the two models discussed above.

B. Numerical solution

In this section we present a numerical solution of our model without the simplification of Sec. III A. The numerical calculation of the Lagrangian multipliers $\nu_1,\ldots,\nu_N$ is limited to relatively short chains, because it involves the solution of N nonlinear equations. Furthermore, closed expressions like Eqs. (13)–(15) for the ensemble averages cannot be calculated. Therefore, we not only have to calculate the Lagrangian multipliers but also the ensemble averages numerically.

To obtain a numerical solution, we rewrite the exponents in Eqs. (2) and (3) as

$$\exp\left(-\frac{1}{l^2}\sum_{n=1}^{N}\nu_n(\mathbf{r}_n-\mathbf{r}_{n-1})^2\right)=\exp\left(-\frac{1}{l^2}\sum_{i,j=0}^{N}a_{ij}\mathbf{r}_i\cdot\mathbf{r}_j\right), \tag{20}$$

where a_{ij} are the components of the tridiagonal matrix

$$\mathbf{A}=\begin{pmatrix} \nu_1 & -\nu_1 & 0 & \ldots & 0 \\ -\nu_1 & \nu_1+\nu_2 & -\nu_2 & \ldots & 0 \\ 0 & -\nu_2 & \nu_2+\nu_3 & \ldots & 0 \\ \vdots & \vdots & \vdots & \ddots & \vdots \\ 0 & 0 & 0 & \ldots & \nu_N \end{pmatrix}. \tag{21}$$

To calculate the partition function, the eigenvectors $\mathbf{b}^k$ and eigenvalues λ_k of the matrix $\mathbf{A}$ are determined. Inserting the expansion $w_n=\Sigma_{k=0}^{N}\chi_k b_n^k$, with $w\in\{x,y,z\}$, into Eqs. (2) and (3), the remaining integrals can easily be calculated, and we obtain the following nonlinear set of equations to determine the Lagrangian multipliers $[\lambda_k=\lambda_k(\{\nu\})]$

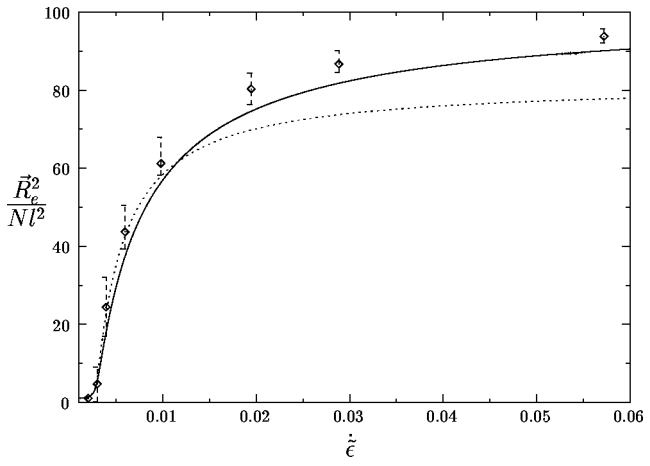

FIG. 5. Elongational rate dependence of the mean square end-to-end distance for an $N=100$ chain calculated numerically with all Lagrangian multipliers (solid curve). The dashed curve again shows the results calculated with only one Lagrangian multiplier. Computer simulation data [16] are provided for comparison (points).

$$\sum_{k=0}^{N}\left(\frac{2}{2\lambda_k+\dot{\tilde{\epsilon}}/2}+\frac{1}{2\lambda_k-\dot{\tilde{\epsilon}}}\right)(b_n^k-b_{n-1}^k)^2=1. \tag{22}$$

Similarly, the end-to-end distance and the radius of gyration are obtained via

$$\langle(\mathbf{r}_N-\mathbf{r}_0)^2\rangle=l^2\sum_{k=0}^{N}\left(\frac{2}{2\lambda_k+\dot{\tilde{\epsilon}}/2}+\frac{1}{2\lambda_k-\dot{\tilde{\epsilon}}}\right)(b_N^k-b_o^k)^2, \tag{23}$$

$$R_G^2=\frac{l^2}{N+1}\sum_{n=0}^{N}\sum_{k=0}^{N}\left(\frac{2}{2\lambda_k+\dot{\tilde{\epsilon}}/2}+\frac{1}{2\lambda_k-\dot{\tilde{\epsilon}}}\right)(b_n^k)^2. \tag{24}$$

The result of the numerical calculation of the strain rate dependence of the mean square end-to-end distance is shown in Fig. 5 for a chain with $N=100$. For low and moderate strain rates, Fig. 5 shows that the mean square end-to-end distance is almost identical to that calculated with the simplification of Eq. (7), but for high strain rates the two curves of Fig. 5 exhibit significant deviations. In contrast to the approximate solution, the end-to-end distance calculated with the Lagrangian multipliers satisfying the exact constraints of Eq. (1) approaches the completely stretched conformation with increasing elongation rate, as it is supposed to. Despite that, our model calculations do not reproduce the simulation data exactly [16]. However, the overall agreement between the two calculations is much better than that achieved with the simplified model. Calculations of the radius of gyration and the intrinsic viscosity yield similar results.

Depending upon the kind of the external field applied to a polymer chain, the Lagrangian multipliers are no longer constant along the chain contour [19], i.e., the bond forces are inhomogeneously distributed along the chain. Figure 6 displays the values of the Lagrangian multipliers as a function of the position along the chain for various strain rates. The values of the Lagrangian multipliers are symmetric with respect to the middle of the chain. Therefore, we only present

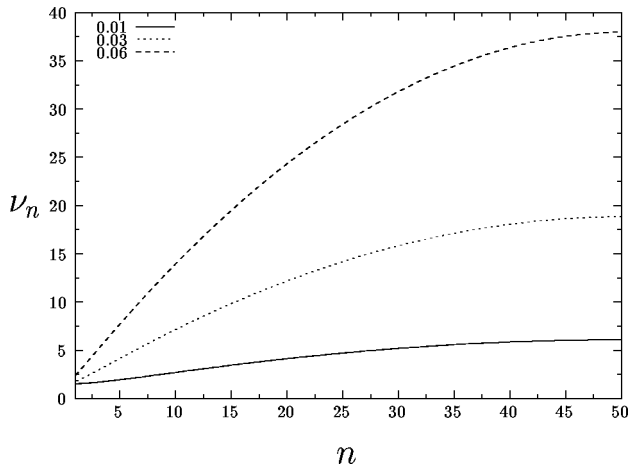

FIG. 6. Values of the Lagrangian multipliers as a function of the position along the chain for different strain rates. The chain lengths is $N=100$. Due to the symmetry, only values up to $N/2$ are presented

values up to $n=N/2$. As is obvious from Fig. 6, the Lagrangian multipliers increase smoothly toward the middle of the chain. The differences between the values of the Lagrangian multipliers at the chain ends and the middle of the chain increase with increasing strain rate, and may differ up to an order of magnitude for very high strain rates. The calculated mean value of all the Lagrangian multipliers along the chain yields good agreement with the single Lagrangian multiplier of the simplified model for all strain rates. The fact that the Lagrangian multipliers in the middle of the chain are larger than those at the chain ends is in agreement with the longer chain segments in the middle of the chain if we use only one Lagrangian multiplier (see Fig. 3).

IV. DYNAMICS

In Sec. III we addressed the steady state properties of a chain in an elongational flow. Now we are interested in the nonequilibrium properties of such a polymer chain. As already mentioned above, the steady state is not always reached in experiments [14,15] because of the limited residence time. In order to provide a theoretical description of experimental data it is necessary to know the residence time dependence of the measured quantities, such as the mean square end-to-end distance, for a given strain rate. For nonequilibrium properties, the initial chain conformation is especially important, because the dynamics of the chain depends upon that conformation [15,16]. Up to now this behavior has only been analyzed by computer simulations of bead-spring and bead-rod models, concentrating primarily on the unraveling behavior of an initially coiled chain [8–10,17,25,26].

As we will demonstrate below, we are able to analyze the nonequilibrium properties of a polymer chain in an external field with our model. In particular, we are able to study the approach of the steady state from any initial conformation. We will, however, only present results for initially coiled and stretched chains, respectively. In this section we will only use the simplified model, i.e., all Lagrangian multiplier are set equal, because the equations are already rather complex with this simplification.

The Hamiltonian for our model, described in Sec. III A, is given by

$$H=\sum_{n=0}^{N}\frac{\mathbf{p}_n^2}{2m}+\frac{\nu}{\beta l^2}\sum_{n=1}^{N}(\mathbf{r}_n-\mathbf{r}_{n-1})^2+V, \tag{25}$$

where V is given by Eq. (5). It should be noted that for nonequilibrium states the Lagrangian multiplier ν depends not only on the strain rate, but also on time. Now $\nu(t)$ has to be determined in such a way that the constant contour length is maintained for every flow strength at any time. Therefore, all averages $\langle\cdots\rangle$ used in this section are ensemble averages at a given time and not time averages.

The dynamics of the polymer chain is described by the well known Langevin equation [22]. Using Hamiltonian (25), we obtain the following $N+1$ coupled equations of motion for the positions of the mass points

$$\zeta\frac{d}{dt}\mathbf{r}_n=\frac{2\nu(t)}{\beta l^2}(\mathbf{r}_{n+1}+\mathbf{r}_{n-1}-2\mathbf{r}_n)+\zeta\boldsymbol{\kappa}\mathbf{r}_n+\boldsymbol{\Gamma}_n(t), \tag{26}$$

where $\boldsymbol{\Gamma}_n(t)$ is a Gaussian distributed random force (white noise). A normal mode transformation according to

$$\mathbf{r}_n(t)=\sqrt{\frac{2}{N+1}}\sum_{k=0}^{N}\boldsymbol{\chi}_k(t)\cos\left[\frac{k\pi}{N+1}\left(n+\frac{1}{2}\right)\right] \tag{27}$$

leads to $N+1$ uncoupled equations for the amplitudes $\boldsymbol{\chi}_k(t)$:

$$\zeta\dot{\boldsymbol{\chi}}_k=\left[-\frac{4\nu(t)}{\beta l^2}\left(1-\cos\frac{k\pi}{N+1}\right)+\zeta\boldsymbol{\kappa}\right]\boldsymbol{\chi}_k+\tilde{\boldsymbol{\Gamma}}_k. \tag{28}$$

The correlations of the transformed random forces $\tilde{\boldsymbol{\Gamma}}_k$ can easily be calculated and we obtain

$$\langle\tilde{\boldsymbol{\Gamma}}_k(t)\rangle=\mathbf{0},$$

$$\langle\tilde{\Gamma}_k^{\alpha}(t)\tilde{\Gamma}_m^{\beta}(t')\rangle=2\zeta k_BT\delta_{km}\delta_{\alpha\beta}\delta(t-t'),\quad \alpha,\beta\in\{x,y,z\}. \tag{29}$$

With the solution of Eq. (28) for the amplitudes $\boldsymbol{\chi}$, the ensemble averages of the end-to-end distance and the radius of gyration can be calculated according to the following equations:

$$\langle[r_{N,\alpha}(t)-r_{0,\alpha}(t)]^2\rangle=\frac{8}{N+1}\sum_{k,m=1,odd}^{N}\langle\chi_k^{\alpha}(t)\chi_m^{\alpha}(t)\rangle\times\cos\frac{k\pi}{2(N+1)}\cos\frac{m\pi}{2(N+1)}, \tag{30}$$

$$R_{G,\alpha}^2=\frac{1}{N+1}\sum_{k=1}^{N}\langle\chi_k^{\alpha}(t)\chi_k^{\alpha}(t)\rangle.$$

The equation to determine the Lagrangian multiplier is given by

$$2\sum_{k=1}^{N}\langle\boldsymbol{\chi}_k(t)\cdot\boldsymbol{\chi}_k(t)\rangle\left(1-\cos\frac{k\pi}{N+1}\right)=Nl^2. \tag{31}$$

The solution of the differential equation (28) is given by

$$\chi_k^{\alpha}(t)=\exp\left(-\int_{t_0}^{t}[\tau_k^{\alpha}(t')]^{-1}dt'\right)\left[\chi_k^{\alpha}(t_0)+\frac{1}{\zeta}\int_{t_0}^{t}dt'\tilde{\Gamma}_k^{\alpha}(t')\exp\left(\int_{t_0}^{t'}[\tau_k^{\alpha}(t'')]^{-1}dt''\right)\right], \tag{32}$$

with

$$\tau_k^{\alpha}(t)=\zeta\left[\frac{4\nu(t)}{\beta l^2}\left(1-\cos\frac{k\pi}{N+1}\right)-\zeta\kappa_{\alpha\alpha}\right]^{-1}. \tag{33}$$

As necessary, the steady state properties (i.e., ν is independent of time, calculated using the above expressions) yield exactly the results presented in Sec. III A.

The equations for the Lagrangian multiplier (4) and the amplitudes χ_k form a nonlinear set of equations, which have to be solved simultaneously. A closed solution of integral (32), however, cannot be given. Hence, we use the following iteration scheme for an approximate solution: For sufficiently small $\Delta t=t-t_0$, the integral over the inverse of the relaxation time can be approximated by $\int_{t_0}^{t}\tau_k^{\alpha}(t')^{-1}dt'\approx\tau_k^{\alpha}(t_0)^{-1}(t-t_0)$. Amplitudes (32) are then given by

$$\chi_k^{\alpha}(t)=\chi_k^{\alpha}(t_0)\exp\left(-\frac{t-t_0}{\tau_k^{\alpha}(t_0)}\right)+\frac{1}{\zeta}\int_{t_0}^{t}dt'\tilde{\Gamma}_k^{\alpha}(t')\times\exp\left(-\frac{t-t'}{\tau_k^{\alpha}(t_0)}\right). \tag{34}$$

The iteration scheme converges in the limit $t-t_0\to 0$. With this approximate solution the following correlations for the amplitudes $\chi_k^{\alpha}(t)$ are obtained:

$$\langle\chi_k^{\alpha}(\tilde{t})\rangle=\langle\chi_k^{\alpha}(\tilde{t}_0)\rangle\exp\left(-\frac{\tilde{t}-\tilde{t}_0}{\tilde{\tau}_k^{\alpha}(\tilde{t}_0)}\right),$$

$$\langle\chi_k^{\alpha}(\tilde{t})\chi_m^{\alpha}(\tilde{t})\rangle=\langle\chi_k^{\alpha}(\tilde{t}_0)\chi_m^{\alpha}(\tilde{t}_0)\rangle\times\exp\left[-(\tilde{t}-\tilde{t}_0)\left(\frac{1}{\tilde{\tau}_k^{\alpha}(\tilde{t}_0)}+\frac{1}{\tilde{\tau}_m^{\alpha}(\tilde{t}_0)}\right)\right]+\tilde{\tau}_k^{\alpha}(\tilde{t}_0)\delta_{km}\left[1-\exp\left(-2\frac{\tilde{t}-\tilde{t}_0}{\tilde{\tau}_k^{\alpha}(\tilde{t}_0)}\right)\right]. \tag{35}$$

In the equations we introduced the scaled time $\tilde{t}=t/\tau$ and relaxation time $\tilde{\tau}_k^{\alpha}=\tau_k^{\alpha}/\tau$, respectively, where τ is defined in Eq. (12). The above correlations together with Eq. (31) provide an iterative solution of the problem, where the iteration process is as follows: First we calculate the Lagrangian multiplier [Eq. (31)] for a given time using Eq. (35). In the next

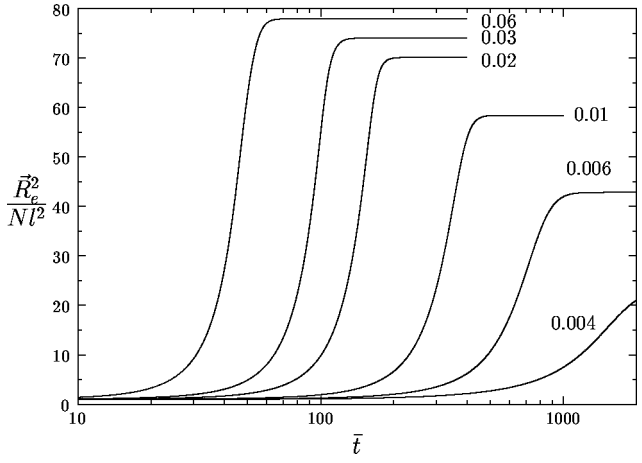

FIG. 7. Mean square end-to-end-distance as a function of time for an initially coiled chain in elongational flow ($N=100$). The various curves correspond to the indicated strain rates.

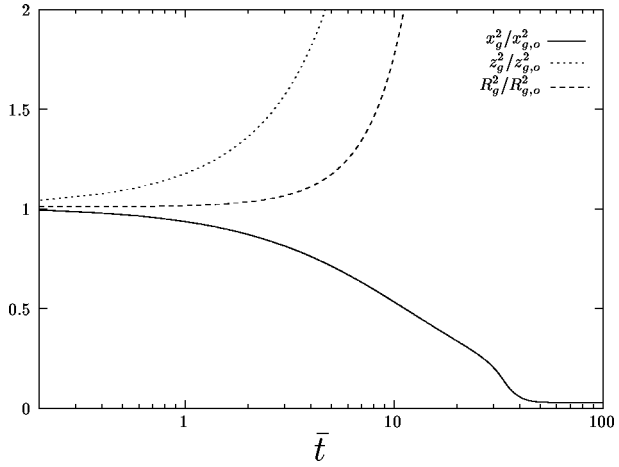

FIG. 8. Radius of gyration (dashed curve) with its components parallel (dotted curve) and perpendicular (solid curve) to the stretching direction.

step all relevant averages, such as the end-to-end distance or the radius of gyration, are calculated for the same time. Finally, the time is increased by one step ($\tilde{t}\rightarrow\tilde{t}+\Delta\tilde{t}$), and the Lagrangian multiplier is calculated again. This procedure is repeated until the stationary state is reached. It should be noted that the dynamics of the system depends on the initial conformation of the polymer chain [$\chi_k^\alpha(t_0)$ appears in the correlations]. Hence in the first step of our iteration scheme the amplitudes $\chi_k^\alpha(t_0)$ at starting time are required. These amplitudes are obtained from the initial chain positions using the following equation:

$$\chi_k^\alpha(\tilde{t}_0)=\sqrt{\frac{2}{N+1}}\sum_{n=0}^{N} r_n^\alpha(\tilde{t}_0)\cos\left[\frac{k\pi}{N+1}\left(n+\frac{1}{2}\right)\right]. \quad (36)$$

With Eq. (36), the initial amplitudes can be calculated for many different chain conformations analytically.

We investigated the dynamics of chains with two distinct initial conformations, namely, initially coiled chains and initially rodlike chains. In each case, the iteration procedure described above worked very well. Figure 7 shows the time dependence of the mean square end-to-end distance for an initially coiled chain for various strain rates. Obviously the end-to-end distance increases with time. In agreement with the steady state results of Fig. 1, significant chain stretching occurs above the critical strain rate $\dot{\tilde{\epsilon}}_c\approx 3\pi^2/N^2$. The various curves of Fig. 7 for the various strain rates display a very similar behavior. For short times (dependent on the strain rate) the end-to-end distance remains virtually constant. After a certain time, the end-to-end distance increases very sharply and approaches the stationary state value, which depends on the strain rate, and which has been already calculated in Sec. III A. Moreover, Fig. 7 shows that the time required to reach the state state decreases with increasing strain rate.

Deeper insight into the conformational changes during the coil-stretch transition can be gained by examining the spatial components of the end-to-end distance and/or the radius of gyration individually. Figure 8 shows the time dependence of the mean square radius of gyration together with its components along the x axis (y axis) and the z axis, respectively. R_G^2 is approximately constant for $\tilde{t}<5$, whereas its x and y components decrease significantly, and the z component increases by a factor of 2. Hence, the even at equilibrium asymmetric coil, with respect to the line connecting the end points of the chain, reorients due to the flow with the major axis of inertia pointing along the flow direction (z direction). Chains close to a smooth surface in a polymer melt exhibit a similar behavior [27]. For $\tilde{t}>7$, the chain rapidly stretches and deforms along the z direction, whereas the transverse components of the radius of gyration decrease to almost zero. Finally, the steady state conformation of the chain is reached. The end-to-end distance exhibits a similar behavior.

In addition, we investigated whether the deformation of the chain in the elongational flow is affine. According to Refs. [26,28], the Henky strain ϵ_f necessary to stretch a chain is given by

$$\epsilon_f=1+\frac{1}{2}\ln N \quad (37)$$

for an affine deformation. The Henky strain ϵ_f is defined as $\epsilon_f=\dot{\epsilon}t_f$. Here t_f is the time where the tangent to the radius of gyration or end-to-end distance curves in Fig. 7 in the steep increasing regime intersects the tangent to the equilibrium value. According to Eq. (37) a Henky strain of approximately $\epsilon_f\approx 3.3$ should be expected for the $N=100$ chain in the case of an affine deformation. In our model we find Henky strains of about 3.3–3.5 depending on the strain rate. This indicates that the chain deformations is affine for most strain rates.

We now examine the time dependence of the end-to-end distance for an initially fully stretched chain. Figure 9 shows that the end-to-end distance decreases monotonically with time. Depending on the strain rate, the chain relaxes, starting at the fully stretched state, to a coiled configuration for low strain rates and partially or almost fully stretched configurations for medium and high strain rates. The end-to-end distances corresponding to this configuration remain constant in time, indicating thermodynamic equilibrium. Similar to the case of the initially coiled chain the time to reach equilib-

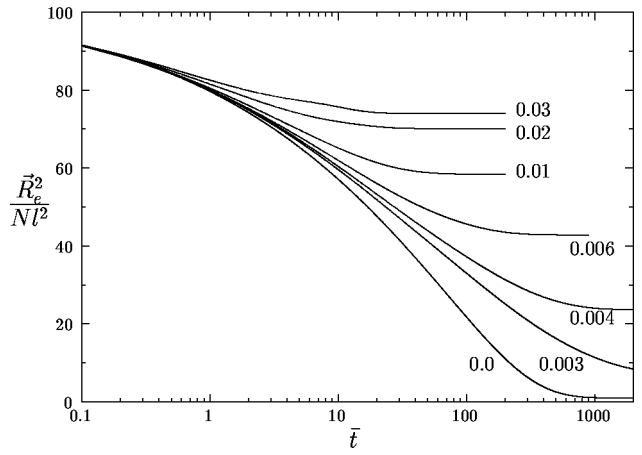

FIG. 9. Decrease of the mean square end-to-end distance with time for different strain rates of an initially fully stretched chain ($N=100$).

rium decreases with increasing strain rate. It should be noted that the equilibrium value of the end-to-end distance is similar to that calculated in Sec. III A or to the value for the initially coiled chain. Thus we do not find any strain rate dependence of the end-to-end distance on the initial configuration of the chain at thermodynamic equilibrium. Calculations with other initial configurations, such as folded chains, exhibit similar results, and again show no dependence on the steady state properties on the specific initial conformation.

V. CONCLUSION

We have analyzed the steady state properties as well as the nonequilibrium dynamic behavior of a polymer chain in an elongational flow using a finite extensible bead spring model. The finite extensibility of the chain is achieved by forcing all the mean square distances between successive points along the chain to assume a constant value. These constraints are taken into account in the solution of the equations of motion by Lagrangian multipliers.

The steady state properties are calculated analytically for a simplified model, where all the Lagrangian multipliers are equal, as well as numerically for the full problem. Depending on the flow strength, the magnitude of the Lagrangian multipliers, and hence the force in a particular bond, depends significantly on its position along the chain.

A comparison of the mean square end-to-end distance obtained from our model with computer simulations for the viscosity exhibits good agreement. This demonstrates that our model captures the main features of polymer chains exposed to an elongational flow.

The investigation of the dynamical behavior of the chains shows that the time to reach the steady state decreases with increasing flow strength. This holds independently of the initial conformation of the chain.

In the present calculations we neglected the hydrodynamic interaction. Considering the qualitative agreement between experimental results and our model calculations, one might argue that the hydrodynamic interaction has only a minor effect on the deformation behavior of a chain. There are, however, certain experimental findings, like the dependence of the relaxation time to approach equilibrium on the initial conformation, which cannot be explained within the current approach. Such effects might be due to the hydrodynamic interaction. Investigations along that line are underway.

[1] A. Peterlin, J. Chem. Phys. **33**, 1799 (1960).
[2] A. Peterlin, Pure Appl. Chem. **12**, 563 (1966).
[3] P.G. DeGennes, J. Chem. Phys. **60**, 5030 (1974).
[4] P. Pincus, Macromolecules **10**, 210 (1977).
[5] R. B. Bird, O. Hassanger, R. C. Armstrong, and C. F. Curtiss, *Dynamics of Polymeric Liquids* (Wiley, New York, 1977), Vol. II.
[6] P. G. DeGennes, *Scaling Concepts in Polymer Physics* (Cornell University, Ithaca, NY, 1979).
[7] H. Yamakawa, *Modern Theory of Polymer Solutions* (Harper and Row, New York, 1971).
[8] J.M. Wiest, L.E. Wedgewood, and R.B. Bird, J. Chem. Phys. **90**, 587 (1989).
[9] J.M. Rallison and E.J. Hinch, J. Non-Newtonian Fluid Mech. **29**, 37 (1988).
[10] E.J. Hinch, J. Non-Newtonian Fluid Mech. **54**, 209 (1994).
[11] P.E. Rouse, J. Chem. Phys. **21**, 1272 (1953).
[12] D. Acierno, G. Titomantio, and G. Marrucci, J. Polym. Sci., Polym. Phys. Ed. **12**, 2177 (1974).
[13] O. Hassager, J. Chem. Phys. **60**, 2111 (1974).
[14] Y. Rabin, F. S. Henyey, and R. K. Pathria, in *Polymer Flow Interactions*, edited by Y. Rabin (AIP, New York, 1985).
[15] T.T. Perkins, D.E. Smith, and S. Chu, Science **276**, 2016 (1997).
[16] U.S. Agarwal, R. Bhargava, and R.A. Mashelkar, J. Chem. Phys. **108**, 1610 (1998).
[17] T.W. Liu, J. Chem. Phys. **90**, 5826 (1989).
[18] H. Haken, *Synergetics*, 3rd ed. (Springer-Verlag, Berlin, 1983).
[19] R.G. Winkler and P. Reineker, Macromolecules **25**, 6891 (1992).
[20] R.G. Winkler, P. Reineker, and L. Harnau, J. Chem. Phys. **101**, 8119 (1994).
[21] R.G. Winkler, L. Harnau, and P. Reineker, Macromol. Theory Simul. **6**, 1007 (1997).
[22] M. Doi and S. F. Edwards, *The Theory of Polymer Dynamics* (Clarendon, Oxford, 1986).
[23] W. Carl, Macromol. Theory Simul. **3**, 705 (1994).
[24] W. Carl and W. Bruns, Macromol. Theory Simul. **3**, 295 (1994).
[25] B.H.A.A. van den Brule, J. Non-Newtonian Fluid Mech. **29**, 37 (1988).
[26] R.G. Larson, Rheol. Acta **29**, 371 (1990).
[27] R.G. Winkler, R. Schmid, A. Gerstmair, and P. Reineker, J. Chem. Phys. **104**, 8103 (1996).
[28] D.F. James and T. Sridhar, J. Rheol. **39**, 713 (1995).